Journal of Materials Chemistry A

Accepted Manuscript

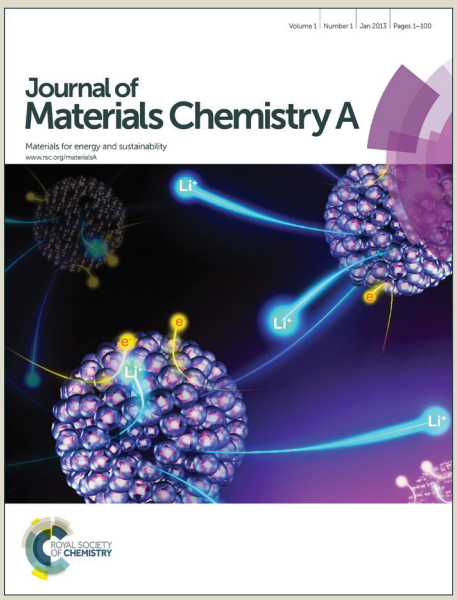

ROYAL SOCIETY OF CHEMISTRY

www.rsc.org/materialsA

Postsynthesis of mesoporous ZSM-5 zeolite by piperidine-assisted desilication and its superior catalytic properties in hydrocarbon cracking

Darui Wang, Lin Zhang, Li Chen, Haihong Wu, Peng Wu*

Shanghai Key Laboratory of Green Chemistry and Chemical Processes, Department of Chemistry, East China Normal University, North Zhongshan Rd. 3663, Shanghai 200062, P. R. China

E-mail: pwu@chem.ecnu.edu.cn

Tel/Fax: 86-21-62232292

Abstract

Mesoporous ZSM-5 zeolites with unique hydrocarbon cracking properties have been postsynthesized from conventional ZSM-5 samples using small molecular organic amine-assisted desilication technique. The parent ZSM-5 zeolites, with regular crystal size of 1 - 2 μm and Si/Al ratios of 15 - 500, were first hydrothermally synthesized using inorganic silicon and aluminum sources and piperidine as structure-directing agent (SDA) with the assistance of active seeds. Controllable mesopores were successfully introduced into as-synthesized ZSM-5 crystals by alkaline-derived desilication with the addition of piperidine or hexamethyleneimine. The addition of organic amines shielded the zeolite crystals from extensive dissolving by NaOH attacking. The mesopores were thus generated controllably within zeolite crystals meanwhile minimizing the loss of microporosity and solid acidity. The incorporation of mesopores made the micropores well interconnected, shortened the average diffusion path lengths as well as maintained more catalytic active sites showing a higher propylene yield and a longer lifetime in the cracking of *n*-hexane.

Keywords:

ZSM-5 zeolite

Piperidine

Mesoporosity

Desilication

n-Hexane cracking

1. Introduction

Crystalline aluminosilicate zeolites possess integral channel systems of well-defined micropores and intrinsic solid acidity. These unique properties endow zeolites with wide applications in the petrochemical industry, such as useful catalysts in the processes of hydrocarbon cracking, alkylation, isomerization and esterification.[1] However, the diffusion limitation and faster catalyst deactivation are the main drawback of microporous zeolites when processing bulky molecules. Their relatively small pores of molecular dimension constrains the diffusion, transportation and access of reactant and product molecules to and from the active sites located inside zeolite channels. Meanwhile, heavy coke will also be easier formed due to low mass transport which lead to faster catalyst deactivation.[2] To overcome these limitations, researchers have focused on the design and synthesis of nanocrystal or hierarchically structured zeolites[3-5] with an improved catalytic performance,[6-9] through shortening the diffusion paths and making more active sites exposed and accessible to gust molecules at the same mass of zeolites.

Synthesizing nanocrystals by altering the crystallization approaches has been proven successful for several zeolite topologies. It is challenging in this respect because the control of crystal size and the separation of nanocrystals from the synthesis mixture are very difficult. Alternatively, the preparation of the zeolites with hierarchical pore structures by pretreatment or post-synthesis has attracted more attentions. Well established methods for incorporating mesoporosity in zeolites include crystallizing zeolites using hard templates like carbon black, carbon

nanotubes, carbon fibers or carbon aerogels[10-12] as as well as soft templates of polydiallyldimethylammonium chloride (PDDA)[13] or silanes.[14-16] The extra voids are created in zeolite matrix after burning off the template species.

The other simple approaches to create mesoporosity within zeolite crystals have been known as post-synthesis treatments such as dealumination and desilication. Under acid or base treatment conditions, the extraction of aluminum and silicon from zeolite framework leads to the formation of structural defects in lattice and then the formation of mesopores. Substantial and tunable mesoporosity can be obtained by varying the concentration of acid or base as well as treatment time and temperature. Dealumination is generally achieved by steam treatment at high temperatures followed by acid leaching, or by using completing agents.[17-18] However, the removal of aluminum inevitably has a negative impact on the zeolite Brønsted acidity. The creation of mesopores by alkaline-assisted desilication has recently received particular attentions because of simplicity and versatility, by which controllable mesopores are incorporated readily into various zeolites, e.g., MFI,[19] BEA,[20] FER,[21] MWW,[22] MOR[23] and AST.[24] This technique preserves better the Brønsted acidity of zeolites in comparison to dealumination. Many alkaline agents (e.g., NaOH, Na_2CO_3, tetrapropylammonium hydroxide, tetrabutylammonium hydroxide) have been employed to remove silicon from zeolite framework.[25] For MFI zeolites, a starting framework with Si/Al ratios of 25 - 50 is optimal for obtaining a substantial intracrystalline mesoporosity together with preserved tetrahedral Al species.[26] When using NaOH alone as an alkaline medium, the kinetic rate of silicon dissolution is

relatively fast, resulting in an uncontrollable formation of mesopores. On the other hand, as desilication extraagents, the quaternary ammonium hydroxides with bulky molecular sizes are less reactive towards silicon dissolution than inorganic hydroxides. The coexistence of quaternary ammonium cations makes the zeolite crystal surface better shielded from the corrosion by NaOH. With combined effects of a high affinity between quaternary ammonium cations and zeolite crystals and the steric hindrance of zeolite micropores to bulky organic species, the desilication process would take place more controllably than the fast silicon dissolution with NaOH alone.[27-29] However, the protective effect is not seen when using the cations that can enter into micropores, e.g. TMA^+ (0.44 nm), which fits within the ZSM-5 micropores (0.56 nm) and cannot offer the same protection to the OH^- attacks as achieved with TPA^+ (0.85 nm) or TBA^+ (1.07 nm).[29] To the best of our knowledge, only few variety of desilication extraagents can offer effective protection. Additional, the price of the teraalkylammonium compounds is high. Therefore, it is desired to develop other effective protecting agents with low cost for preparing the hierarchical zeolites with tunable mesoporosity in the industrial case.

Here, we disclose a method for incorporating mesoporousity into ZSM-5 zeolites using NaOH solution using cyclic amines like piperidine as mesopore-directing agents for the first time. Moreover, the parent ZSM-5 zeolites were also skillfully hydrothermally synthesized from an inorganic silica source with piperidine as SDA. The mesoporous ZSM-5 zeolites prepared by desilication in the NaOH/piperidine system proved to be highly efficient for hydrocarbon cracking.

2. Experimental

2.1. Materials

All chemicals and reagents were obtained from commercial supplier and used without further purification: tetraethyl orthosilicate (Sigma-Aldirich, ≥98% Reagent Grade), tetrapropylammonium hydroxide (TCI, 25 wt% in water), colloidal silica (Sigma-Aldirich, 30 wt% suspension in water), piperidine (Aladdin, ≥99.5% analytical standard), aluminum sulfate octadecahydrate (Aladdin, 98.0%–102.0% ACS reagent), sodium hydroxide (Alfa Aesar, 98.0% flake) , ammonium chloride (Alfa Aesar, ≥98%).

2.2. Synthesis of ZSM-5 zeolites

The active seeding gel was prepared according to the procedures reported previously.[30] Tetraethyl orthosilicate (TEOS) as silica source was dropped into an aqueous solution of 25 wt% tetrapropylammonium hydroxide (TPAOH) under stirring. After homogenizing at 353 K for 2 h, the synthetic gel, with a molar composition of TEOS: 0.15TPAOH: $14H_2O$, was transferred into a Teflon-lined steel autoclave and aged at 393 K for 3 h. After cooling, the obtained homogeneous mixture was used as seeding gel directly in the synthesis of ZSM-5 zeolites without further treatment.

In the synthesis of ZSM-5 zeolites, piperidine (PI) and colloidal silica (30 wt% of SiO_2) were employed as SDA and silica source, respectively. The molar ratios of PI/Si and H_2O/Si were 0.5 and 25, respectively. Aluminum sulfate and sodium hydroxide were first dissolved in aqueous solution of PI. After stirring for 30 minutes, silica sol and active seeding gel were dropped into the solution in sequence. The SiO_2 in active

seeding gel corresponded to 1 wt% of total SiO_2 in synthetic system, while the Si/Al molar ratio was varied in the range of 15 - 500, and the Na/Si ratio was fixed at 0.5. After stirring for another 30 minutes, the mixture was charged into an autoclave where the crystallization was carried out at 443 K for 72 h. The product was collected by filtration followed by washing with distilled water several times, dried at 373 K overnight, and then calcined in air at 823 K for 6 h to remove the organic template. The zeolites were converted into ammonium form via conventional ion-exchange with ammonium chloride solution at 353 K for 2 h, and finally into proton type by calcination at 823 K for 6 h.

2.3. Alkaline treatment

The calcined Na-ZSM-5 zeolite with a Si/Al ratio of 40 was subjected to desilication by alkaline treatment under stirring (500 rpm) at liquid-to-solid ratio of 50 mL to 1.0 g. The treatment was carried out in an aqueous NaOH solution or the mixture of NaOH and PI or hexamethyleneimine (HMI) at the temperature of 338 K for 30 min. Afterwards, the zeolite suspension was cooled down in ice-bath, filtered and washed with deionized water until the pH value below 9. The zeolites were converted to proton type via ion-exchange and calcination following the same procedures mentioned above. The samples prepared by alkaline treatment were denoted as AT *m* - PI *n* or AT *m* - HMI *n*, where *m* represents the molar concentration of NaOH and *n* indicates the molar ratio of piperidine or hexamethyleneimine to SiO_2 in zeolites.

2.4. Characterization methods

Powder X-ray diffraction (XRD) was employed to check the structure and crystallinity of the zeolites. The XRD patterns were collected on a Rigaku Ultima IV diffractometer using Cu Kα radiation at 35 kV and 25 mA in the 2θ angle range of 5 - 35º using a step size of 0.04° and at a scanning speed of 10°/min. The relative crystallinity was calculated by comparing the area of the five peaks between 2θ= 22.5º and 25.0º of alkaline treated samples to that for the parent ZSM-5. Nitrogen gas adsorption measurements were carried out at 77 K on a BEL-MAX gas/vapor adsorption instrument. The samples were evacuated at 573 K for at least 6 h before adsorption. The *t*-plot method was used to discriminate between micro- and mesoporosity. The surface areas were calculated by the Brunauer-Emmett-Teller (BET) method. The mesopore size distribution was obtained by the BJH model from the adsorption branches of the isotherms. Si and Al contents were determined by inductively coupled plasma emission spectrometry (ICP) on a Thermo IRIS Intrepid II XSP atomic emission spectrometer. The IR spectra were collected on a Nicolet Nexus 670 FT-IR spectrometer in absorbance mode at a spectral resolution of 2 cm^{-1}. The sample was pressed into a self-supported wafer with 4.8 mg cm^{-2} thickness, which was set in a quartz cell sealed with CaF_2 windows and connected to a vacuum system. After evacuated at 723 K for 2 h, pyridine adsorption was carried out by exposing the pretreated wafer to a pyridine vapor at 298 K for 0.5 h. The adsorbed pyridine was evacuated successively at 423 K for 1 h. The spectra were collected at room temperature. Acidity was measured by temperature-programmed desorption of ammonia (NH_3-TPD) with a Micrometrics tp-5080 equipment equipped with a

thermal conductivity detector (TCD) detector. Typically, 100 mg of sample was pretreated in helium stream (30 mL min^{-1}) at 823 K for 1 h. The adsorption of NH_3 was carried out at 323 K for 1 h. The sample was flushed with helium at 373 K for 2 h to remove physisorbed NH_3 from the catalyst surface. The TPD profile was recorded at a heating rate of 10 K min^{-1} from 373 K to 873 K. Scanning electron microscopy (SEM) was performed on a Hitachi S-4800 microscope to determine the crystal morphology. Transmission electron microscopy (TEM) images were collected on a Tecnai G^2 F30 microscope after the samples were deposited onto a holey carbon foil supported on a copper grid. ^{27}Al solid-state MAS NMR spectra were recorded on a VARIAN VNMRS-400WB spectrometer under one pulse condition. The spectra were recorded at a frequency of 104.18 MHz, a spinning rate of 9.0 kHz, and a recycling delay of 4 s. $KAl(SO_4)_2 \cdot 12H_2O$ was used as the reference for chemical shift.

2.5. Catalytic cracking of n-hexane

The cracking of *n*-hexane was performed using a continuous flow system in a fixed-bed quartz reactor (i.d. 25 mm). The H-ZSM-5 catalyst in the reactor was pretreated in a dry N_2 flow at 873 K for 1 h, and then the reactor was cooled to the reaction temperatures (723 - 873 K). The reaction was carried out under atmospheric pressure using N_2 as a carrier gas. The typical catalyst loading and flow rate of N_2 carrier were 0.3 g and 30 mL min^{-1}, respectively. The weight hourly space velocity of *n*-hexane (WHSV) was varied from 2 h^{-1} to 25 h^{-1}. The reaction products were analyzed by an on-line gas chromatograph with an FID detector and equipped with an Al_2O_3/S capillary column (50 m × 0.53 mm × 0.25 μm). The amount of coke formed

during the reaction was determined from the weight loss from 673 to 1073 K in a thermogravimetric (TG) profile, which was collected on a thermogravimetric differential thermal analyzer (Mettler-Toledo, TG-DTA-851^e).

3. Results and discussion

3.1. Physicochemical properties of parents and alkaline treated ZSM-5 zeolites

The parent ZSM-5 samples were synthesized at different Si/Al molar ratios of 15 - 500. With the presence of active seeding gel and piperidine as SDA, all samples exhibited typical and well-resolved diffractions due to MFI structure (Fig. 1). No impurities or amorphous phase were detected in XRD patterns. For comparison, the samples with a Si/Al molar ratio of 40 were synthesized in the absence of active seeding gel or piperidine under otherwise the same conditions. They turned to be amorphous phase or less crystalline ZSM-5 zeolites (see ESI, Fig. S1), indicating that active seeding gel and piperidine both played important roles in the crystallization of ZSM-5. The active seeding gel served as the nuclei for zeolite crystal growth with cooperative structure-direction functionality of piperidine molecules. The results are fully in agreement to the synthesis of TS-1 in system of hexamethyleneimine/active seeds.[31] To obtain highly crystalline ZSM-5 zeolites, not a single one can be dispensable for active seeding gel and piperidine.

The scanning electron microscopy (SEM) images showed that the ZSM-5 zeolites synthesized at different Si/Al molar ratios displayed well defined crystal morphologies that varied with Si/Al molar ratio (Fig. 2). The morphology changed from spherical aggregated of nanocrystals for the sample of Si/Al = 15 to approximate

cubic particles for the sample of Si/Al = 500. The samples prepared at Si/Al ratios of 40 and 100 showed uniform cross-shaped and cuboid particles, respectively. All samples displayed highly regular crystal sizes of 1 - 2 μm.

The ZSM-5 zeolite synthesized at Si/Al of 40 was used as the parent sample for investigating the effects of desilication conditions on the zeolite structure and mesopore formation. The XRD pattern of the parent zeolite exhibited the MFI structure with a relatively high crystallinity (Fig. 3a). The desilication performed in NaOH only led to a severe destruction of zeolite framework, giving rise to a AT 0.2 sample showing the diffractions with greatly decreased intensities (Fig. 3a). In contrast to desilication with NaOH alone, the treatment in the mixture of NaOH and piperidine destructed the zeolite framework slightly, as the intensities of the characteristic diffractions attributed to the MFI topology increased with an increasing amount of piperidine (Fig. 3b-f). Obviously, piperidine added in NaOH solution was protective to the zeolite structure. Similar results have been reported for the desilication with a mixture of NaOH and bulky tetrapropylamine hydroxide. It is well known that the high affinity of TPA^+ for the zeolite combined with its intrinsic steric hindrance slow down the kinetics of the desilication process.[29, 32]

The parent ZSM-5 presented a type I isotherm of N_2 adsorption, characteristic of microporosity (Fig. 4A). Its micropore volume (0.16 $cm^3\ g^{-1}$) and specific surface area (S_{BET} of 316 $m^2\ g^{-1}$) were comparable to that of ZSM-5 zeolites reported in literature. The parent ZSM-5 was subjected to the treatment with 0.2 M NaOH at 338 K for 30 min, that is, under standard treatment conditions widely used.[33] The resulting samples

showed multilayer adsorption natures in the P/P_0 range of 0.5 - 0.99, and the isotherms changed to combined ones of type I and type IV (Fig. 4A). This was indicative of the formation of a hierarchical porous system consisting of microporosity and mesoporosity. As shown in Table 1, the desilication made the mesopore surface area and mesopore volume increase from 12 to 149 $m^2 g^{-1}$ and from 0.05 to 0.57 $cm^3 g^{-1}$, respectively. Meanwhile, the micropore volume decreased from 0.16 to 0.11 $cm^3 g^{-1}$, implying the increase of mesopore surface area by10 folds was accompanied by sacrificing 30% of micropore volume. The Si/Al molar ratio detected by ICP in the resulting solid decreased from 36 for parent ZSM-5 (40) to 16 for the AT 0.2 sample prepared by the NaOH treatment only (Table 1). Mesopore formation is presumed to be due to the OH^- assisted selective extraction of framework silicon.[26] The yield of the AT 0.2, defined as grams of solid after workup per gram of parent sample was 41%, meaning that the framework species, mainly silicon, were dissolved into the solution by 60%.

In contrast to desilication with NaOH, the treatment of with the mixture of NaOH and piperidine minimized the loss of microporosity in zeolites while created an extensive mesoporosity. Fig. 5 shows the changes of product yield, crystallinity, introduced mesopore surface area and remaining micropore volume as a function of the piperidine amount added in NaOH treatment. The solid yield, crystallinity and remaining micropore volume showed a progressive increase with an increasing piperidine/zeolite ratio, whereas the mesopore surface area introduced showed a volcano curve. At a low piperidine concentration, the mesopore surface area reached

240 and 220 m^2 g^{-1} for AT 0.2 - PI 0.01 and AT 0.2 - PI 0.02, respectively (Table 1). The values of mesopore volume were also higher than that of AT 0.2. Moreover, in the presence of piperidine, the micropore volume was higher (0.13 cm^3 g^{-1}) than that in the absence of piperidine (0.11 cm^3 g^{-1}) (Table 1). At higher piperidine concentrations, the values of S_{meso} and V_{meso} of AT 0.2 - PI 0.03 and AT 0.2 - PI 0.04 were lower in comparison to AT 0.2, and they still possessed the well preserved micropore volumes, higher relative crystallinity (> 70%) and higher solid yields (> 80%). Nevertheless, the AT 0.2 - PI 0.05 sample prepared at piperidine/zeolite ratio of 0.05 almost did not gain the mesopores. This sample had high solid yield of 96% and relative crystallinity of 83%, demonstrating that only a little amount of silicon was extracted by NaOH treatment. This supported the hypothesis that addition of piperidine protected the zeolite crystal against an extensive OH^- attack and prevented a massive dissolution of the zeolite framework. The limited or controlled silicon leaching with the addition of piperidine also brought difference in the size of the mesopores created. A spectacular difference could be seen between the hierarchical zeolite prepared by treatment in pure NaOH solution (20 - 30 nm) and that obtained in a mixture of NaOH and piperidine (10 - 13 nm) (Fig. 4B). The existence of piperidine had the advantages of narrowing the mesopore size distribution as well as achieving smaller mesopores.

The transmission electron microscopy provided the mesoporosity-related information in agreement with the abovementioned gas-adsorption analyses. The parent microporous ZSM-5 zeolite showed a dark image (Fig. 6a) and displayed an ordered arrangement of micropores without interruption in a wide area (Fig. 6b). The

TEM image densities of NaOH or NaOH/piperidine-treated zeolites became lower as a result desilication (Fig. 6c and e). An obvious difference in mesopore size and regularity was observable between AT 0.2 and AT 0.2 - PI 0.02, The former hierarchical zeolite prepared by NaOH treatment only conatined the mesopores of 20 - 30 nm (Fig. 6d), whereas the latter obtained and the assistance of piperidine had more regular mesopores of 10 - 13 nm (Fig. 6f). Fig. 7 shows the SEM images of NaOH-treated ZSM-5. The morphology differed between the NaOH-treated ZSM-5 and NaOH/piperideine-treated ZSM-5 (Fig. 7a-d). Obviously, the crystals in AT 0.2 were destroyed seriously mostly because of a non protective desilication (Fig. 7a). With the co-existence of piperidine, the morphology was well maintained after the NaOH treatment. In particular, the AT 0.2 - PI 0.05 sample had a morphology highly resembling the untreated sample (Fig. 7d), indicating that the desilication almost did not occur. The result was in agreement with the textural properties shown above.

The desilication of ZSM-5 was also investigated with the mixture of NaOH and piperidine at various OH^- concentrations (0.1 and 0.5 M) and various amounts of piperidine. As expected, the treatment with 0.1 M NaOH resulted in only a little increase in mesopore volume (Table 1). The SEM images showed that there was no difference in crystallite shape between parent ZSM-5 and AT 0.1 (Fig. 7e). The desilication in a more concentrated NaOH (0.5 M) and piperidine mixture did not make the pore diameter smaller when comparing with NaOH treatment only. It is noteworthy that such a high alkali concentration diminished the micropore volume and lowered the solid yield seriously in comparison to diluted solution of 0.2 M

NaOH (Table 1). According, the morphology of zeolite was destroyed extensively in 0.5 M NaOH solution only (Fig. 7f) or adding the piperidine as protective agent (we did not show here).

The ZSM-5 zeolites with Si/Al molar ratios of 15, 50, 100 and 500 were also treated using 0.2 M NaOH (AT 0.2) and the mixture of NaOH and piperidine (AT 0.2 -PI 0.02). Fig. 8 shows the dependence of solid yield, crystallinity, increased mesopore surface area and of micropore volume on the Si/Al molar ratio. The AT 0.2 - PI 0.02 samples always had a higher solid yield and a higher crystallinity than the AT - 0.2 ones. Moreover, more mesopore surface area was created and more micropore volume was preserved with the addition of piperidine when the desilication performed on the ZSM-5 zeolites with different Si/Al molar ratios. The mesopore surface area developed upon alkaline treatment showed a volcano change with Al content, with the maximums appearing in the optimum Si/Al molar ratio range of 25 - 50. These results were fully in agreement with the report that the key factor to introduce mesopores into ZSM-5 by NaOH desilication is to use the zeolites with the Si/Al molar ratios of 25 - 50.[26] At low Si/Al molar ratios, the framework Al with a high content would protect the silicon atoms against leaching by NaOH, and then only a small fraction of mesopores were formed. On the other hand, for the zeolites with higher Si/Al molar ratios, an extensive dissolution of bulky crystals took place easily in NaOH solution, leading to a low solid yield, e.g. only 20- 30% for ZSM-5 (500) even when the protective agent of PI was co-added. In this case, the large cavities with a low contribution to mesopore surface area were formed. Fig. 9 showed the SEM images of

ZSM-5 with different Si/Al ratios after treated using NaOH only (AT 0.2) or using the mixture of NaOH and piperidine (AT 0.2 - PI 0.02). The morphology of NaOH-treated ZSM-5 (15) was similar to that of the parent, whereas the morphology of ZSM-5 (500) was destroyed seriously by desilication. Independent of Si/Al ratios, the AT 0.2 - PI 0.02 samples preserved more completely the crystal morphology in comparison to the AT 0.2 samples as a result of protective desilication in the presence of piperidine.

3.2 Solid acidity and of mesoporous ZSM-5 zeolites

The zeolite acidity was investigated by NH_3-TPD and FT-IR spectroscopy. Fig. 10 shows the NH_3-TPD profiles of the parent ZSM-5 and alkali-treated samples both in proton form. The low temperature peak (400 - 575 K) was caused by the desorption of ammonia adsorbed on weak Brønsted (BAS) and Lewis (LAS) acid sites. The high temperature peak (575 - 800 K) corresponds to the NH_3 desorption from catalytically active BAS and LAS with stronger acidity.[34, 35] After the parent ZSM-5 was desilicated with alkaline solution, the high-temperature peak intensity became lower, whereas the low-temperature peak became boarded. It implied that the catalytically active BAS and LAS were partially destroyed by desilication. The broadening of the low-temperature peak could be a result of forming extra-framework Al species with a weak Lewis acidity. Both desilication and dealumination of framework Al to extra-framework Al probably took place under current alkaline treatment condition. Fortunately, when the parent ZSM-5 was desilicated with the mixture of NaOH and piperidine, the high-temperature peak was largely maintained, and its intensity was increased with increasing the piperidine amount. As shown in Table S1 in ESI, the

total acid quantity of the parent ZSM-5 was approximately 0.47 mmol g^{-1}, all alkaline-treated samples showed higher total acid quantity due to the decrease of Si/Al. However, the strong acid quantity of the AT -0.2 decreased to 0.15 mmol g^{-1}, about 46% of strong acid sites were destroyed when compared to that of the parent ZSM-5 (0.28 mmol g^{-1}). Fortunately, we could obtain higher strong acid quantity of 0.19 mmol g^{-1} and 0.25 mmol g^{-1} for AT 0.2 - PI 0.01 and AT 0.2 - PI 0.02, respectively. Thus, adding a suitable amount of piperidine in NaOH solution not only introduced the mesopores into zeolite crystals but also well preserved the strong acid sites.

In order to further investigate the acidic properties of zeolites, FT-IR spectra of adsorbed pyridine and ^{27}Al MAS NMR spectra were measured for the parent ZSM-5 and alkali-treated samples. Fig. 11 shows the FT-IR spectra after removing physical adsorption of pyridine molecules on the parent and alkali-treated samples. The stretching bands of pyridinium ion at around 1450 and 1540 cm^{-1} were attributed to LAS and BAS, respectively.[36] The amount of BAS was slightly decreased by alkaline desilication in comparison to the parent samples, regardless of using NaOH only or the mixture of NaOH and piperidine. In contrast, the amount of LAS was increased by alkaline treatment probably as a result of extra-framework Al formation. Nevertheless, the desilication with piperidine/NaOH solution made the BAS remain more.

The parent ZSM-5 showed in ^{27}Al MAS NMR spectrum only a resonance of tetrahedral Al (58 ppm) with that of octahedral Al (0 ppm) was almost absent (Fig. 12a), indicating that all Al atoms were present in the framework position.[37] The desilication developed the octahedral species showing an obvious resonance at 0 ppm,

and caused that of tetrahedral Al broader in comparison to the parent sample (Fig. b-d). These results indicated that the dealumination of framework Al to extra-framework species occurred during the alkaline treatment, and that the coordination states of Al became less symmetric. Nevertheless, the NMR spectra indicated again the co-addition of piperidine in NaOH solution was useful to maintain more tetrahedral Al species in that framework against a deep dealumiantion.

The FT-IR spectrum of alkali-treated sample (AT 0.2 - PI 0.05) showed the bands at 2800 - 3000 cm^{-1} (ESI, Fig. S2b), which are assigned to the C-H stretching vibrations of the piperidine molecules.[38] These organic species-related bands, absent in the spectrum of the parent ZSM-5 sample (ESI, Fig. S2a), should be due to the piperidine molecules incorporated into ZSM-5 channels or on the crystal external surface. These piperidine molecules could protect the surrounding framework silicon from an extensive crystal dissolving, leading to a more controllable desilication. The band at 1100 cm^{-1} is assigned to Si-O-Si vibration, and the bands at 550 cm^{-1} and 450 cm^{-1} for all samples is assigned to the asymmetric stretching mode of five-ring in the MFI framework and the Si-O bending mode, respectively.[39] These band remained unchanged for the AT 0.2 - PI 0.05 sample, indicating it was highly ordered in crystalline structure.

Our results clearly showed the desilication kinetics were relatively slower by the mixure of NaOH and piperidine in comparison to using NaOH only. The aluminosilicate framework was better shielded from a deep and uncontrollable attacking by OH^- with the addition of piperidine. As a consequence, a large amount of

mesopores with smaller diameter could be introduced into zeolite crystals while minimizing the loss of micropores and gaining a higher solid yield in the mixture of piperidine and NaOH. In addition, more catalytically active sites were maintained as well.

The protected desilication has been realized by the addition of piperidine. Thus, we have also attempted the introduction of mesopores with hexamethyleneimine (HMI), a similar secondary amine to piperidine but having a more bulky molecular size. The desilication with the addition of HMI was carried out under the same conditions as piperidine. The textural parameters of the zeolites (AT 0.2 - HMI 0.01, AT 0.2 - HMI 0.02) and solid yield were similar to those of AT 0.2 - PI 0.01 and AT 0.2 - PI 0.02 (Table 1), respectively. Thus, a protective desilication could be achieved with HMI. We also conducted the treatment with other organic bases, such as piperazine and ethylenediamine anhydrous. Unfortunately, these amines did not serve as protection agents as HMI and PI in desilication.

The protective desilication mechanism of piperidine or hexamethyleneimine could be a little different from that of using TPAOH or TBAOH.[29] With larger ionic dimensions than the ZSM-5 micropores (0.56 nm), tetrapropylammonium (TPA^+, 0.85 nm) and tetrabutylammonium (TBA^+, 1.07 nm) can block the pore entrance, and their intrinsic steric hindrance then slows down the kinetics of the desilication process. However, piperidine or hexamethyleneimine molecules, smaller than the ZSM-5 micropore size, can enter into zeolites channels readily and they offer the same protection to the OH^- attacking as achieved with TPA^+ or TBA^+. Piperidine was

employed as the structure-directing agents in the hydrothermal synthesis of ZSM-5 zeolites in this study. In post-treatment with NaOH solution, the same zeolite structure still could distinguish piperidine or hexamethyleneimine at molecular level. Those accommodated amine molecules then acted as efficient pore-growth moderators during desilication.

It is worth noting that the amount of piperidine added influenced the mesopore formation. As illustrated in Fig. 13, the optimal formation of mesopores in zeolite crystals by desilication depends on the amount of piperidine and controlled dissolution of zeolite crystal. Evidently, at a low piperidine concentration, no protection is guaranteed. Extra mesopores are then extensively developed with a significant loss of micropore volume, as in the case of AT 0.2 sample. In the opposite extreme, at high piperidine concentration, the zeolite crystals are overprotected against silicon leaching by NaOH, leading to a high solid yield and only a small proportion of mesopores. Only when using an optimal amount of piperidine in the middle, a balance between the piperidine protection and dissolution of zeolite crystal is realized, introducing a large amount of mesopores into zeolites while preserving the maximum micropore volume.

3.3 Catalytic cracking of n-hexane over parent and alkaline treated H-ZSM-5 zeolites

The catalytic cracking of *n*-hexane was carried out using the parent ZSM-5 and those samples obtained by alkaline treatment with the addition of various amounts of piperidine. The influence of reaction temperature on the catalytic performances was investigated at 723 - 873 K (Fig. 14A). The conversion of *n*-hexane increased along

with raising the reaction temperature for each catalyst. The catalytic cracking of *n*-hexane over H-ZSM-5 was not limited by the diffusion of *n*-hexane under the present reaction conditions as reported previously.[40] AT 0.2 and AT 0.2 - PI 0.02 exhibited lower conversions than the parent at a low reaction temperature of 723 K. The conversions at low temperature were decreased with a decrease in the amount of BAS according to the high-temperature peak intensity of NH_3-TPD shown in Fig. 10. These findings suggested that catalytic cracking of *n*-hexane occurred mainly on BAS at low temperature. However, AT 0.2 - PI 0.02 showed higher conversions than the parent at higher temperatures (> 773 K), suggesting that both BAS and LAS would contribute to the catalytic cracking of *n*-hexane under these conditions. Similar results were also reported by Mochizuki et al.[41]

Secondary, the product distribution was also investigated at 723 - 873 K (Fig. 14B). For all the catalysts, the selectivities to ethylene and C_6^+ were increased along with the reaction temperature, while the selectivities to propene and butenes were decreased. According to above results, C_6^+ was formed by a successive reaction of propylene and butenes. At a high temperature, primary carbenium ions would be easier to produce, and ethylene would be formed not only by cracking of *n*-hexane but also by successive reactions of C_4 or C_4^+. Therefore, the selectivity of ethylene would be enhanced at higher temperatures.

The selectivity of propylene of alkali-treated samples was higher than that of the parent. Hydrogen transfer index (HTI) is a parameter measuring the hydrogen transfer activity of the catalyst during cracking reactions.[42] It is defined as the ratio of sum of

propane and butanes selectivity to propylene and butenes selectivity. The parent showed the highest HTI compared with AT 0.2 and AT 0.2 - PI 0.02 (Fig. 15A). Propylene yield was significantly high for alkali-treated samples because of their significantly low hydrogen transfer activity. The secondary reactions were suppressed predominantly due to shorter residence time, and a rapid elution of primary reaction products was realized by introducing extensive mesopores into alkali-treated samples. As shown in Fig. 14B, the coke amounts formed on alkali-treated samples were lower than that of the parent because of the former possessed a shortened diffusion path length. That coke precursors could easily diffuse out of the micropores, suppressing the formation of heavy coke inside micripores and mesopores.

In order to clarify the effect of mesopores introduced into zeolites on deactivation rate, the changes in the conversion along with the time-on-stream were examined at 873 K with a higher WHSV of 25 h^{-1} (Fig. 16). The initial conversions for the parent, AT 0.2 and AT 0.2 - PI 0.02 were 75, 74 and 62%, respectively. The initial conversion of AT 0.2 was the lowest, because the catalytically active BAS on the alkali-treated ZSM-5 were seriously removed by the desilication and dealumination. Fortunately, catalytically active BAS on the AT 0.2 - PI 0.02 were retained with the addition of piperidine during alkaline treatment. On the other hand, in the alkali-treated catalysts, the coke precursors and the other products could easily diffuse out of the micropores. The coke formation was effectively prevented as shown in Table S2 in ESI, and then the deactivation was mitigated. This result was caused by the shorter diffusion path length in the alkali-treated catalysts.

Conclusion

The ZSM-5 zeolites with different Si/Al molar ratios of 15 - 500 and crystal diameters of 1 - 2 μm can be hydrothermally synthesized using piperidine as the structure-directing agent with the assistant of active seeds and alkali metal ions. Hierarchical zeolites combining microporosity and mesoporosity together are readily postsynthesized by the desilication of as-synthesized ZSM-5 in NaOH solution or the mixture of NaOH with piperidine or hexamethyleneimine. The zeolites are better shielded from the attacking by OH^- with the addition of cyclic secondary amines. As a consequence, mesopores with smaller diameters could be introduced into ZSM-5 crystals while minimizing the loss of micropores and catalytically active sites. Possessing a lower hydrogen transfer activity, the alkali-treated ZSM-5 samples show a significantly higher propylene yield in the cracking of *n*-hexane than the parent ZSM-5. The mesopore formation suppresses effectively the secondary reactions and coke formation, leading to a longer catalyst life.

Acknowledgement

We gratefully acknowledge the National Natural Science Foundation of China (21373089), PhD Programs Foundation of Ministry of Education (2012007613000), the National Key Technology R&D Program (2012BAE05B02), and the Shanghai Leading Academic Discipline Project (B409).

References

1 A. Corma, *Chem. Rev*., 1995, **95**, 559-614.

2 A. Corma, *Chem. Rev*. 1997, **97**, 2373-2419.

3 L. Tosheva and V. P.Valtchev, *Chem. Mater*., 2005, **17**, 2494-2513.

4 A. Corma, V. Fornes, S. B. Pergher, T. L. M. Maesen and J. G. Buglass, *Nature*, 1998, **396**, 353-356.

5 C. Madsen and C. J. H. Jacobsen, *Chem. Commun*. 1999, **8**, 673-674.

6 M. E. Davis, *Nature*, 2002, **417**, 813-821.

7 Y. Song, X. Zhu, Y. Song and Q. Wang, *Appl. Catal., A*, 2006, **302**, 69-77.

8 L. Zhao, B. Shen, J. Gao and C. Xu, *J. Catal*., 2008, **258**, 228-234..

9 J. Kim, M. Choi and R. Ryoo, *J. Catal*., 2010, **269**, 219-228.

10 C. J. H. Jacobsen, C. Madsen, J. Houzvicka, I. Schmidt and A. Carlsson, *J. Am. Chem. Soc*., 2000, **122**, 7116-7117.

11 I. Schmidt, A. Boisen, E. Gustavsson, K. Stahl, S. Pehrson, S. Dahl, A. Carlsson and C. J. H. Jacobsen, *Chem. Mater*., 2001, **13**, 4416-4418.

12 Y. Tao, H. Kanoh and K. Kaneko, *J. Am. Chem. Soc*., 2003, **125**, 6044-6045.

13 F. S. Xiao, L. Wang, C. Yin, K. Lin, Y. Di, J. Li, R. Xu, D. S. Su, R. Schlögl, T. Yokoi and T. Tatsumi, *Angew. Chem. Int. Ed*., 2006, **45**, 3090-3093.

14 H. Wang and T. J. Pinnavaia, *Angew. Chem. Int. Ed*., 2006, **45**, 7603-7606.

15 M. Choi, H. S. Cho, R. Srivastava, C. Venkatesan, D. H. Choi and R. Ryoo, *Nat. Mater*., 2006, **5**, 718-723.

16 Z. Zhao, Y. Liu, H. Wu, X. Li, M. He and P. Wu, *J. porous. Mater*., 2010, **17**, 399-408.

17 S. V. Donk, A. H. Janssen, J. H. Bitter and K. P. Jong, *Catal. Rev*., 2003, **45** 297-319.

18 C. S. Triantafillidis, A. G. Vlessidis and N. P. Evmiridis, *Ind. Eng. Chem. Res*., 2000, **39**, 307-319.

19 J. C. Groen, J. C. Jansen, J. A. Moulijn and J. Pérez-Ramírez, *J. Phys. Chem., B*, 2004, **108**, 13062-13065.

20 J. C. Groen, S. Abello, L. A. Villaescusa and J. Pérez-Ramírez, *Microporous Mesoporous Mater*., 2008, **114**, 93-102.

21 A. Bonilla, D. Baudouin and J. Pérez-Ramírez, *J. Catal*., 2009, **265**, 170-180.

22 Ł. Mokrzycki, B. Sulikowski and Z. Olejniczak, *Catal. Lett*., 2009, **127**, 296-303.

23 J. C. Groen, T. Sano, J. A. Moulijn and J. Pérez-Ramírez, *J. Catal*., 2007, **251**, 21-27.

24 J. Pérez-Ramírez, S. Abello, L. A. Villaescusa and A. Bonilla, *Angew. Chem. Int. Ed*., 2008, **47**, 7913-7917.

25 J. C. Groen, L. A. A. Peffer, J. A. Moulijn and J. Pérez-Ramírez, *Microporous Mesoporous Mater*., 2004, **69**, 29-34.

26 J. C. Groen, L. A. A. Peffer, J.A. Moulijin and J. Pérez-Ramírez, *Chem. Eur. J*., 2005, **11**, 4983-4994.

27 K. Sadowska, A. Wach, Z. Olejniczak, P. Kuśtrowski and J. Datka, *Microporous Mesoporous Mater*., 2013, **167**, 82-88.

28 D. Verboekend and J. Pérez-Ramírez, *Chem. Eur. J*., 2011, **17**, 1137-1147.

29 J. Pérez-Ramírez, D. Verboekend, A. Bonilla and S. Abello, *Adv. Funct. Mater*., 2009, **19**, 3972-3979.

30 D. Wang, L. Xu and P. Wu, *J. Mater. Chem., A*, 2014, **2**, 15535-15545.

31 H. Zhang, Y. Liu, H. Wu, Y. Jiang, L. Chen, M. He and P. Wu, *Chem. Lett*., 2006, **35**, 1276-1277

32 S. Abelló, A. Bonilla, and J. Pérez-Ramírez, *Appl. Catal., A*, 2009, **364**, 191-198.

33 J. C. Groen, J. A. Moulijin and J. Pérez-Ramírez, *J. Mater. Chem*., 2006, **16**, 2121-2131.

34 M. E. Franke and U. Simon, *Chem. Phy. Chem*., 2004, **5**, 465-472.

35 K. Suzuki, Y. Aovagi, N. Katada, M. Choi, R. Ryoo and M. Niwa, *Catal. Today*., 2008, **132**, 38-45.

36 E. P. Parry, *J. Catal*., 1963, **2**, 371-379.

37 C. Fernandez, I. Stan, J. -P. Gilson, K. Thomas, A. Vicente, A. Bonilla and J. Pérez-Ramírez, *Chem. Eur. J*., 2010, **16**, 6224-6233

38 E. Gornicka, J. E. Rode, E. D. Raczynska, B. Dasiewicz and J. C. Dobrowolski, *Vibrational Spectroscopy*, 2004, **36** 105-115.

39 D. Lesthaeghe, P. Vansteenkiste, T. Verstraelen, A. Ghysels, C. E. A. Kirschhock, J. A. Martens, V. V. Speybroeck and M. Waroquier, *J. Phys. Chem. C*, 2008, **112**, 9186-9191.

40 H. Mochizuki, T. Yokoi, H. Imai, R. Watanabe, S. Namba, J. N. Kondo and T. Tatsumi, *Microporous Mesoporous Mater*., 2011, **145**, 165-171.

41 H. Mochizuki, T. Yokoi, H. Imai, S. Namba, J. N. Kondo and T. Tatsumi, *Appl. Catal., A*, 2012, **449**, 188-197.

42 X. Zhu, S. Liu, Y. Song and L. Xu, *Appl. Catal., A*, 2005, **288**, 134-142.

Figure captions

Fig. 1. XRD patterns of ZSM-5 synthesized at a Si/Al molar ratio of 15 (a), 30 (b), 40 (c), 50 (d), 100 (e), 200 (f) and 500 (g).

Fig. 2. SEM images of ZSM-5 synthesized at a Si/Al molar ratio of 15 (a), 40 (b), 100 (c) and 500 (d).

Fig. 3. XRD patterns of parent ZSM-5 (a) and alkaline-treated samples of AT 0.2 - PI 0.05 (b), AT 0.2 - PI 0.04 (c), AT 0.2 - PI 0.03 (d), AT 0.2 - PI 0.02 (e), AT 0.2 - PI 0.01 (f) and AT 0.2 (g).

Fig. 4. Fig. 4. N_2 isotherms (A) and BJH pore size distributions (B) of parent ZSM-5(a) and alkali-treated samples of AT 0.2 - PI 0.03 (b), AT 0.2 - PI 0.02 (c), AT 0.2 - PI 0.01 (d) and AT 0.2 (e).

Fig. 5. Dependence of product yield (A), relative crystallinity (B), introduced mesopore surface area (C) and micropore volume (D) on the molar ratio piperidine/ZSM-5(40).

Fig. 6. TEM images of parent ZSM-5 (a, b), and alkaline-treated samples of AT 0.2 (c, d) and AT 0.2 - PI 0.02 (e, f).

Fig. 7. SEM images of ZSM-5(40) after alkaline treatment with various OH^- concentrations and piperidine amount. AT 0.2 (a), AT 0.2 - PI 0.01 (b), AT 0.2 - PI 0.03 (c), AT 0.2 - PI 0.05 (d), AT 0.1 (e) and AT 0.5 (f).

Fig. 8. Dependence of the textural properties of the zeolites treated with AT 0.2 (solid square) and AT 0.2 - PI 0.02 (hollow square) conditions on the Si/Al molar ratio: the yield (A), the crystallinity (B), the increase in introduced mesopore surface area (C) and the decrease in preserved volume of micropore (D).

Fig. 9. SEM images of ZSM-5 synthesized with a Si/Al molar ratio of 15(a, b), 100 (c,

d) and 500 (e, f) treated by 0.2 M NaOH in the absence of piperidine (AT 0.2, a, c, e) and treated by 0.2 M NaOH in the presence of piperidine (AT 0.2 -PI 0.02, b, d, f).

Fig. 10. NH_3-TPD profiles of parent ZSM-5 (a), AT 0.2 - PI 0.02 (b), AT 0.2 - PI 0.01 (c), AT 0.2 (d). All samples were of proton-form.

Fig. 11. Pyridine-adsorption FT-IR spectra of parent ZSM-5 (a), AT 0.2 - PI 0.02 (b), AT 0.2 - PI 0.01 (c), AT 0.2 (d). All samples were of proton-form.

Fig. 12. ^{27}Al MAS NMR spectra of parent ZSM-5 (a), AT 0.2 - PI 0.02 (b), AT 0.2 - PI 0.01 (c), AT 0.2 (d). All samples were of proton-form.

Fig. 13. Graphic illustration for the desilication and mesopore formation of ZSM-5 crystals in alkaline treatment with different addition amount of piperidine.

Fig. 14. Conversion (A) and product distribution (B) of *n*-hexane cracking over different catalysts: parent ZSM-5 (a), AT 0.2 (b) and AT 0.2 - PI 0.02 (c). Reaction conditions: 0.3 g catalyst, WHSV = 2 h^{-1}, TOS = 10 h.

Fig. 15. HTI (A) and coke amount (B) of *n*-hexane cracking over different catalysts: parent ZSM-5 (a), AT 0.2 (b) and AT 0.2 - PI 0.02 (c). Reaction conditions: 0.3 g catalyst, WHSV = 2 h^{-1}, TOS = 10 h.

Fig. 16. Change in the conversion with time on stream of *n*-hexane cracking over different catalysts: parent ZSM-5 (a), AT 0.2 (b) and AT 0.2 - PI 0.02 (c). Reaction conditions: 0.1 g catalyst, WHSV = 25 h^{-1}, 873 K.

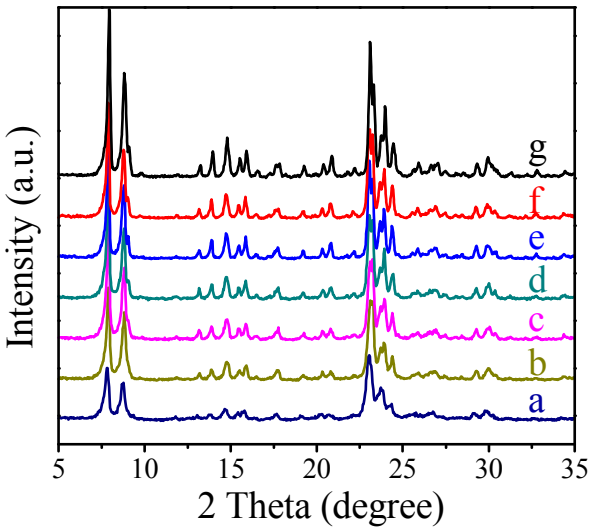

Fig. 1. XRD patterns of ZSM-5 as-synthesized at a Si/Al molar ratio of 15 (a), 30 (b), 40 (c), 50 (d), 100 (e), 200 (f) and 500 (g) in the presence of active seeding gel and piperidine.

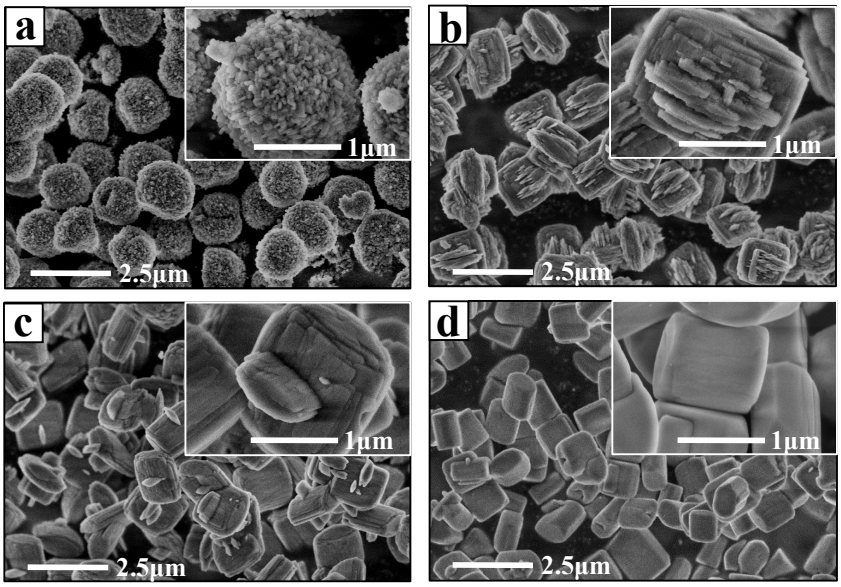

Fig. 2. SEM images of ZSM-5 synthesized at a Si/Al molar ratio of 15 (a), 40 (b), 100 (c) and 500 (d).

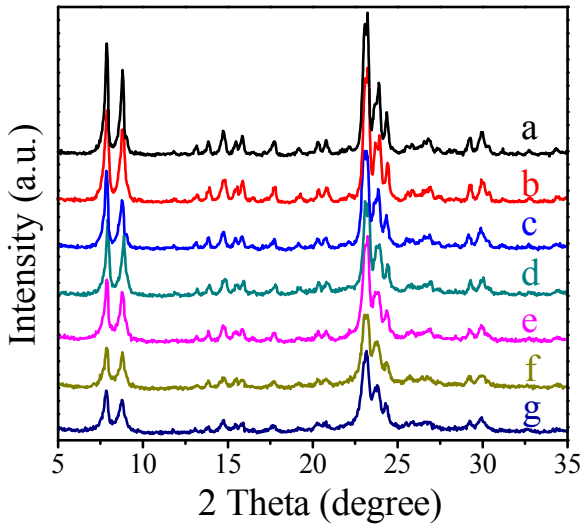

Fig. 3. XRD patterns of parent ZSM-5 (Si/Al = 40) (a), and alkaline-treated samples of AT 0.2 - PI 0.05 (b), AT 0.2 - PI 0.04 (c), AT 0.2 - PI 0.03 (d), AT 0.2 - PI 0.02 (e), AT 0.2 - PI 0.01 (f) and AT 0.2 (g).

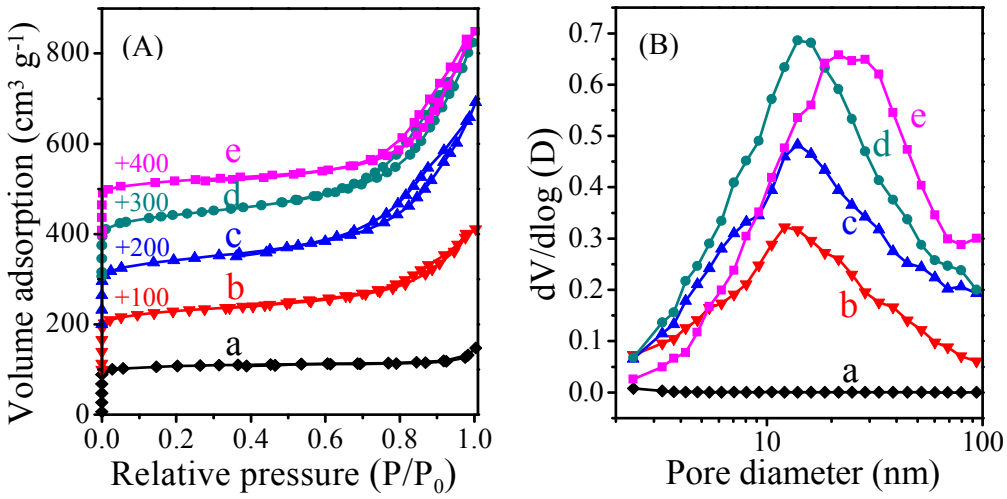

Fig. 4. N_2 isotherms (A) and BJH pore size distributions (B) of parent ZSM-5(a) and alkali-treated samples of AT 0.2 - PI 0.03 (b), AT 0.2 - PI 0.02 (c), AT 0.2 - PI 0.01 (d) and AT 0.2 (e).

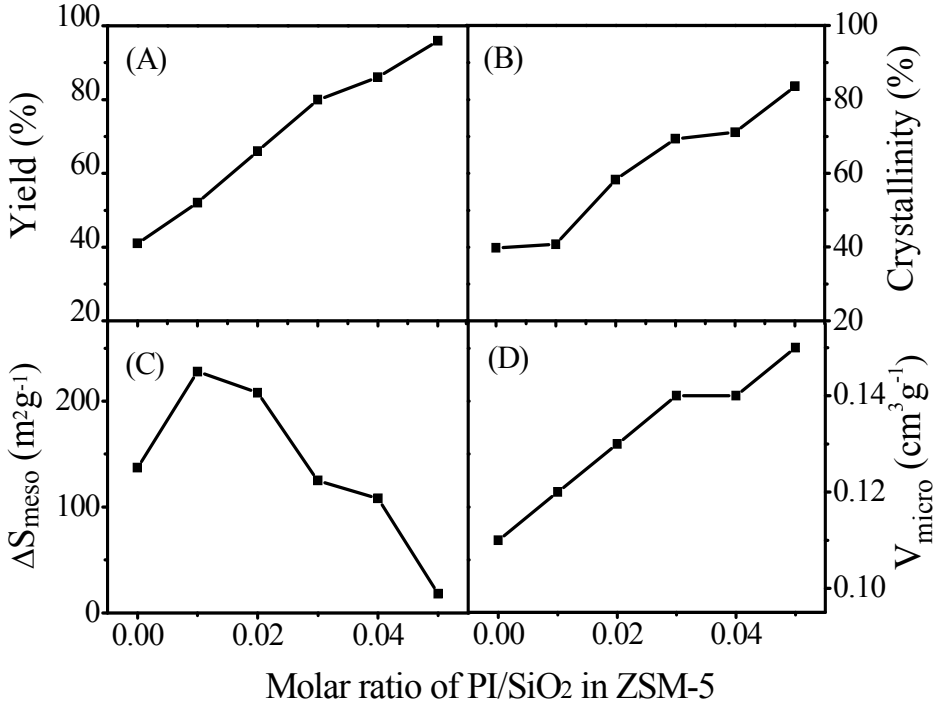

Fig. 5. Dependence of product yield (A), relative crystallinity (B), introduced mesopore surface area (C) and micropore volume (D) on the molar ratio piperidine/SiO_2 in ZSM-5(40).

Table 1 Chemical composition and textural properties of the parent and alkali-treated ZSM-5 zeolites

Samples	NaOH (M)	Amine/SiO_2[a]	Yield[b] (%)	Bulk Si/Al[c]	V_{meso}[d] ($cm^3\ g^{-1}$)	S_{BET}[e] ($m^2\ g^{-1}$)	S_{meso}[f] ($m^2\ g^{-1}$)	V_{micro}[f] ($cm^3\ g^{-1}$)	V_{total}[g] ($cm^3\ g^{-1}$)
ZSM-5 (40)	-	-	100	36	0.05	316	12	0.16	0.21
AT 0.1	0.1	-	78	28	0.28	350	84	0.12	0.40
AT 0.1 - PI 0.01	0.1	0.01	85	32	0.25	221	74	0.14	0.39
AT 0.2	0.2	-	41	16	0.56	364	149	0.11	0.67
AT 0.2 - PI 0.01	0.2	0.01	52	21	0.68	487	240	0.12	0.80
AT 0.2 - PI 0.02	0.2	0.02	66	26	0.59	452	220	0.13	0.72
AT 0.2 - PI 0.03	0.2	0.03	80	33	0.33	420	137	0.14	0.47
AT 0.2 - PI 0.04	0.2	0.04	86	33	0.29	370	120	0.14	0.43
AT 0.2 - PI 0.05	0.2	0.05	96	35	0.06	296	30	0.16	0.22
AT 0.2 - HMI 0.01	0.2	0.01	54	23	0.61	435	226	0.12	0.73
AT 0.2 - HMI 0.02	0.2	0.02	63	25	0.56	408	140	0.13	0.69
AT 0.5	0.5	-	22	8	0.66	378	239	0.08	0.74
AT 0.5 - PI 0.02	0.5	0.02	30	12	0.43	369	164	0.11	0.54
AT 0.5 - PI 0.04	0.5	0.04	39	16	0.44	332	121	0.12	0.56
AT 0.5 - PI 0.08	0.5	0.08	46	19	0.43	284	101	0.12	0.55
P (15)	-	-	100	12	0.13	303	63	0.15	0.28
AT 0.2	0.2	-	86	11	0.23	336	113	0.13	0.36
AT 0.2 - PI 0.02	0.2	0.02	91	12	0.29	381	129	0.13	0.42
ZSM-5 (50)	-	-	100	43	0.14	382	23	0.16	0.30
AT 0.2	0.2	-	40	20	0.55	403	206	0.12	0.67
AT 0.2 - PI 0.02	0.2	0.02	62	30	0.63	468	235	0.14	0.76
ZSM-5 (100)	-	-	100	92	0.10	352	44	0.17	0.27
AT 0.2	0.2	-	34	37	0.31	380	170	0.11	0.42
AT 0.2 - PI 0.02	0.2	0.02	52	53	0.40	387	137	0.13	0.53
ZSM-5 (500)	-	-	100	321	0.05	302	26	0.17	0.22
AT 0.2	0.2	-	22	86	0.12	323	80	0.11	0.23
AT 0.2 - PI 0.02	0.2	0.02	32	128	0.21	361	110	0.12	0.33

[a] The molar ratio of PI or HMI/SiO_2 in zeolite.

[b] The solid product yield obtained after workup.

[c] Given by ICP analysis.

[d] $V_{meso} = V_{total} - V_{micro}$.

[e] Obtained by BET method.

[f] Obtained by *t*-plot method.

[g] Given by the adsorption amount at $P/P_0 = 0.99$.

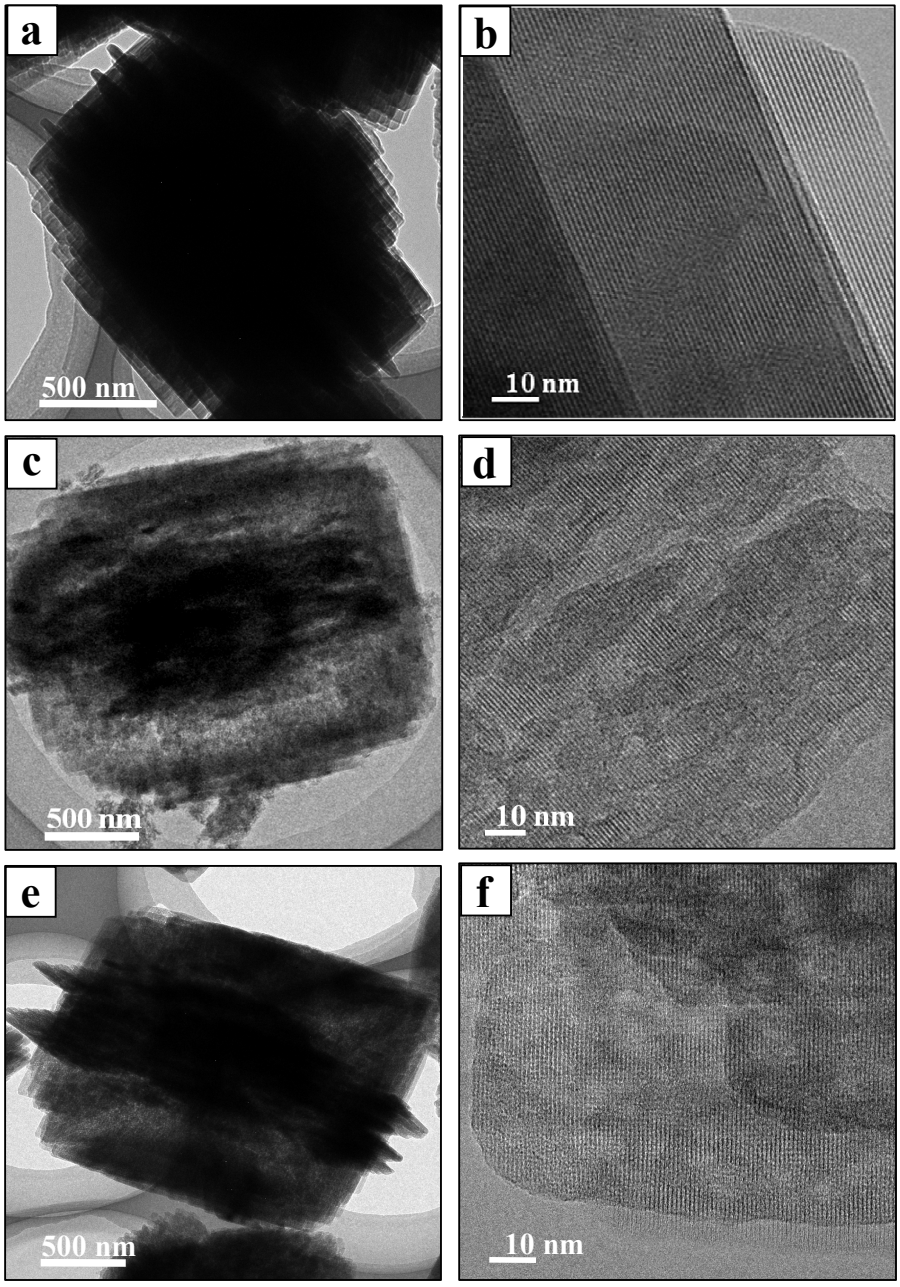

Fig. 6. TEM images of parent ZSM-5 (a, b), and alkaline-treated samples of AT 0.2 (c, d) and AT 0.2 - PI 0.02 (e, f).

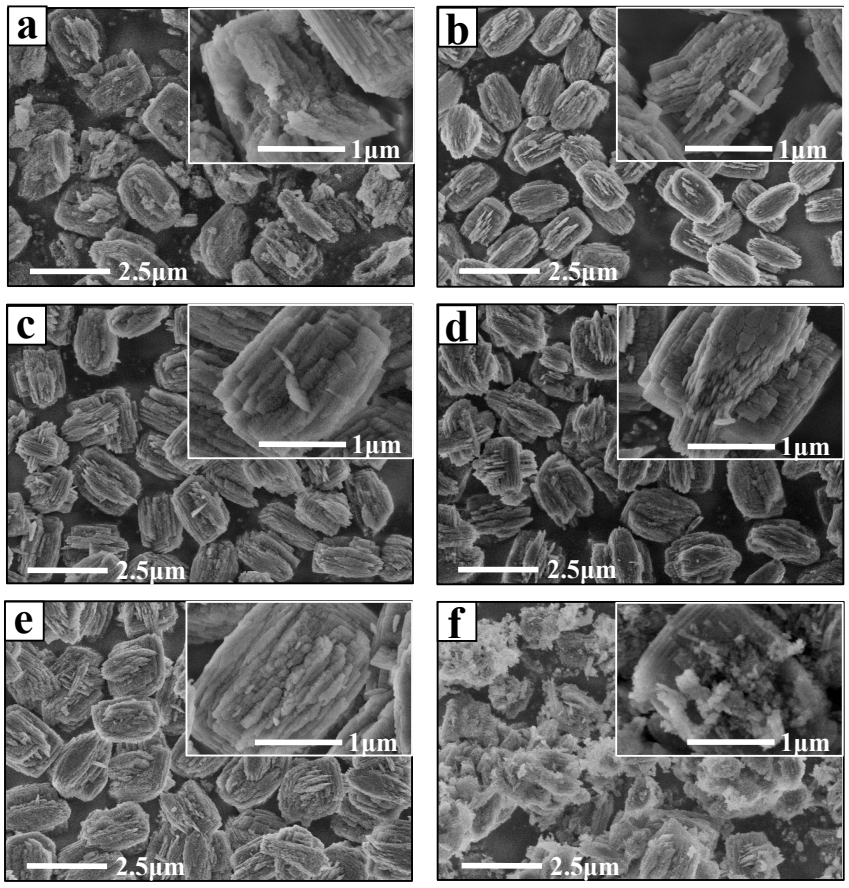

Fig. 7. SEM images of ZSM-5(40) after alkaline treatment with various OH^- concentrations and piperidine amount. AT 0.2 (a), AT 0.2 - PI 0.01 (b), AT 0.2 - PI 0.03 (c), AT 0.2 - PI 0.05 (d), AT 0.1 (e) and AT 0.5 (f).

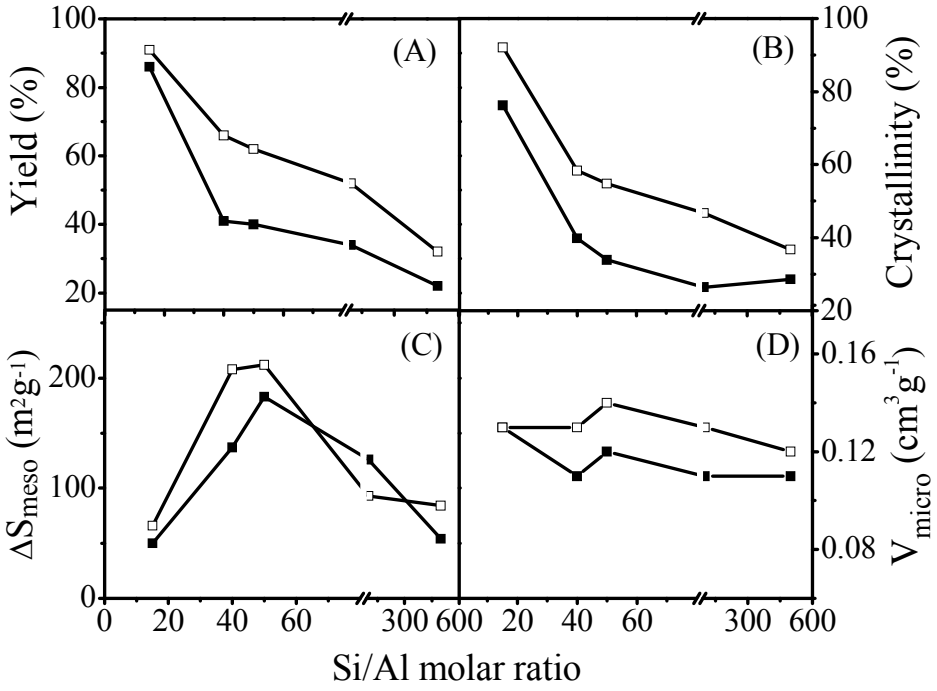

Fig. 8. Dependence of the textural properties of the zeolites treated with AT 0.2 (solid square) and AT 0.2 - PI 0.02 (hollow square) conditions on the Si/Al molar ratio: the yield (A), the crystallinity (B), the increase in introduced mesopore surface area (C) and the decrease in preserved volume of micropore (D).

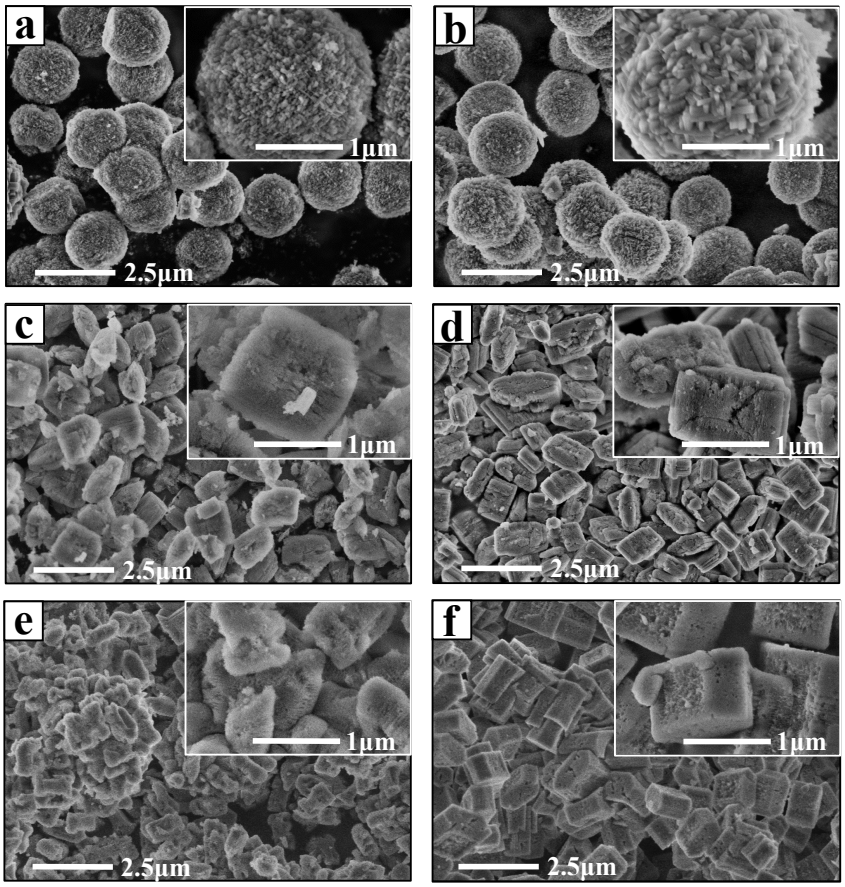

Fig. 9. SEM images of NaOH-treated ZSM-5 as-synthesized at a Si/Al molar ratio of 15 (a, b), 100 (c, d) and 500 (e, f) either in the absence of piperidine (AT 0.2, a, c, e) or in the presence of piperidine (AT 0.2 -PI 0.02, b, d, f).

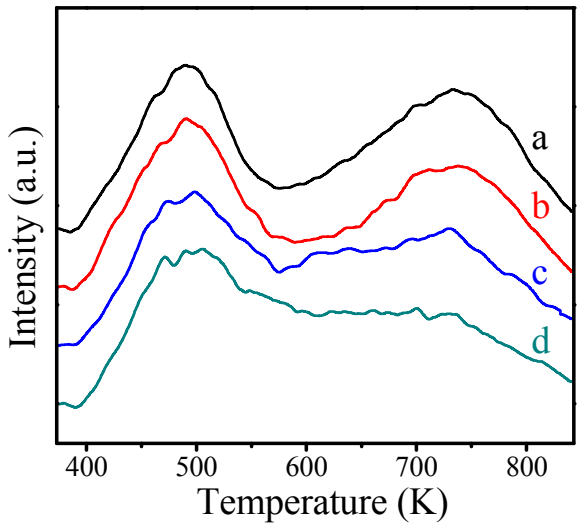

Fig. 10. NH_3-TPD profiles of parent ZSM-5 (a), AT 0.2 - PI 0.02 (b), AT 0.2 - PI 0.01 (c), AT 0.2 (d). All samples were of proton-form.

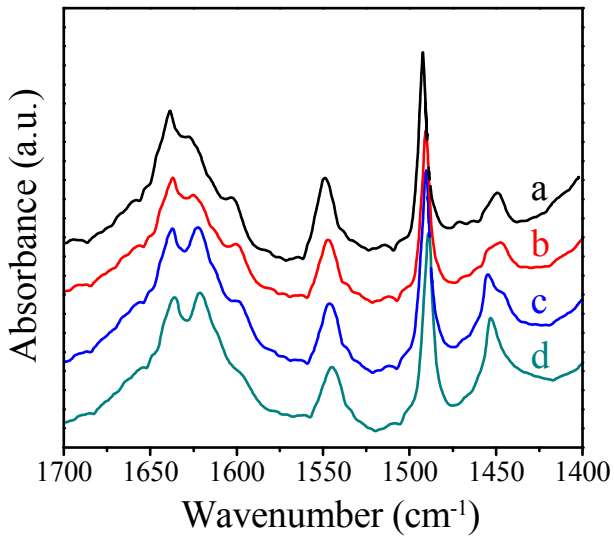

Fig. 11. Pyridine-adsorption FT-IR spectra of parent ZSM-5 (a), AT 0.2 - PI 0.02 (b), AT 0.2 - PI 0.01 (c), AT 0.2 (d). All samples were of proton-form.

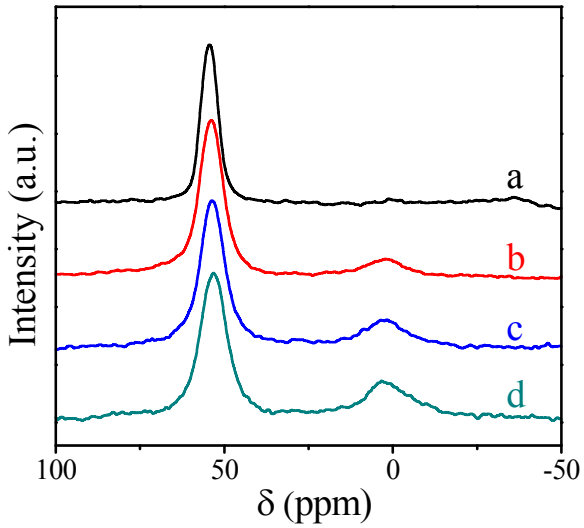

Fig. 12. ^{27}Al MAS NMR spectra of parent ZSM-5 (a), AT 0.2 - PI 0.02 (b), AT 0.2 - PI 0.01 (c), AT 0.2 (d). All samples were of proton-form.

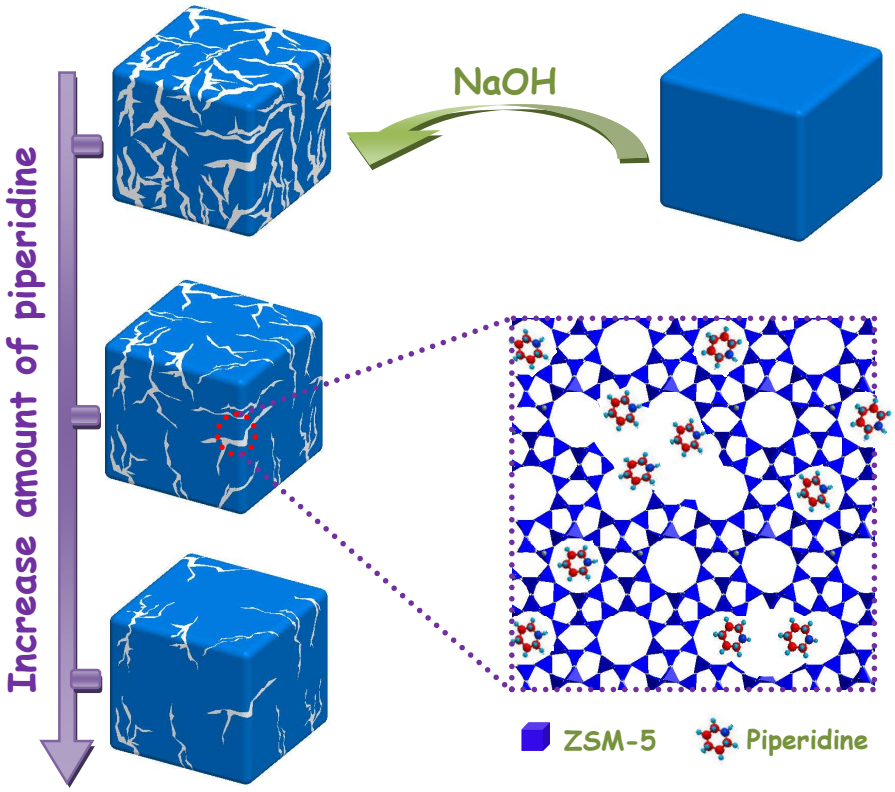

Fig. 13. Graphic illustration for the desilication and mesopore formation of ZSM-5 crystals in alkaline treatment with different addition amount of piperidine.

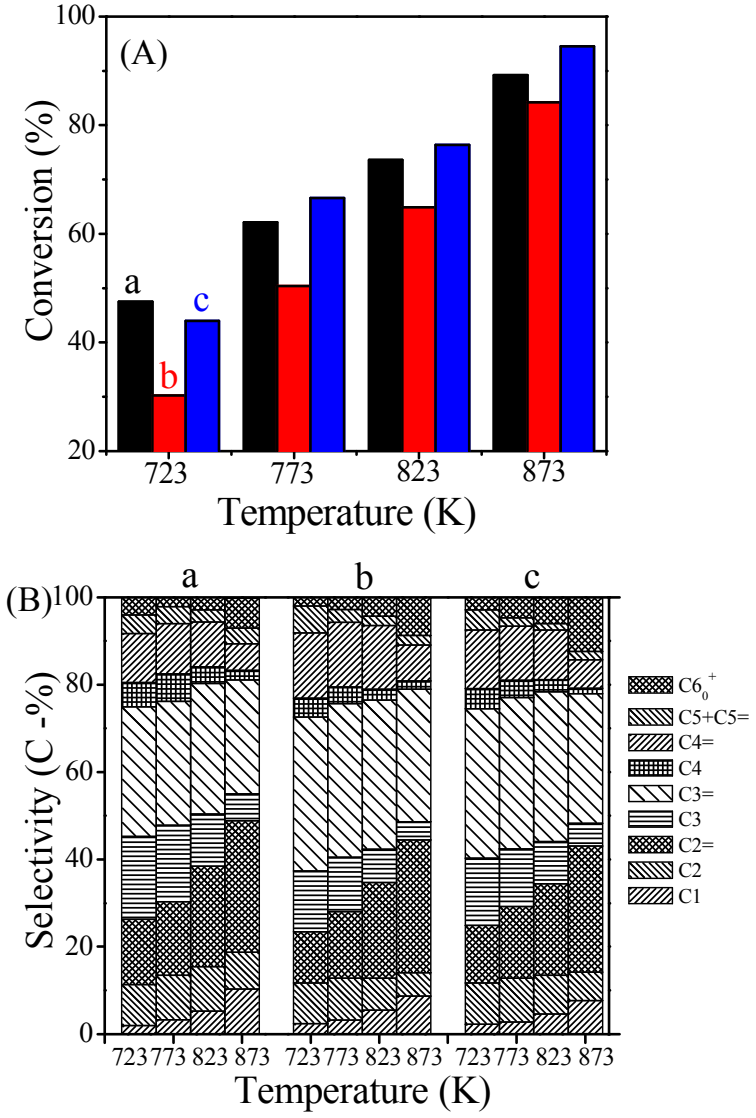

Fig. 14. Conversion (A) and product distribution (B) of *n*-hexane cracking over different catalysts: parent ZSM-5 (a), AT 0.2 (b) and AT 0.2 - PI 0.02 (c). Reaction conditions: 0.3 g catalyst, WHSV = 2 h^{-1}, TOS = 10 h.

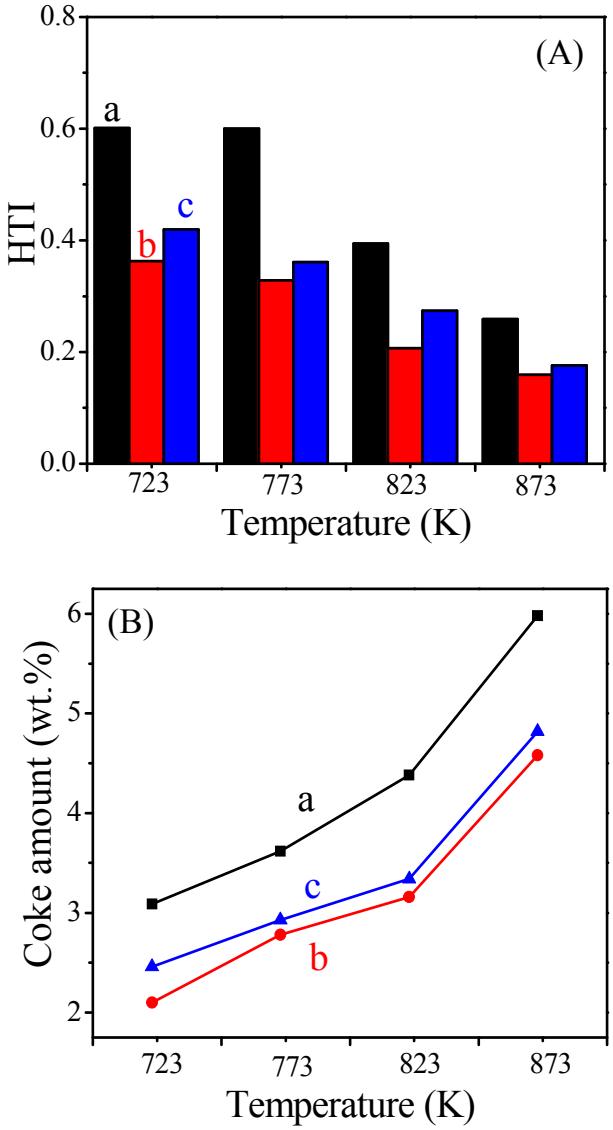

Fig. 15. HTI (A) and coke amount (B) of *n*-hexane cracking over different catalysts: parent ZSM-5 (a), AT 0.2 (b) and AT 0.2 - PI 0.02 (c). Reaction conditions: 0.3 g catalyst, WHSV = 2 h^{-1}, TOS = 10 h.

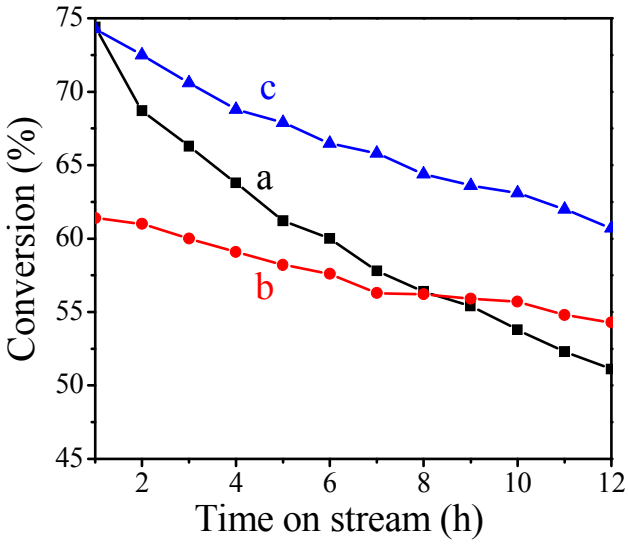

Fig. 16. Change in the conversion with time on stream of *n*-hexane cracking over different catalysts: parent ZSM-5 (a), AT 0.2 (b) and AT 0.2 - PI 0.02 (c). Reaction conditions: 0.1 g catalyst, WHSV = 25 h^{-1}, 873 K.

Graphic Abstract